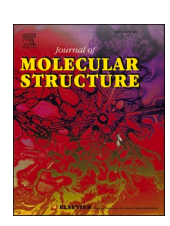
ELSEVIER

Contents lists available at ScienceDirect

Journal of Molecular Structure

journal homepage: www.elsevier.com/locate/molstr



Acetylplatinum(II) complexes containing PTA-derived ligands: Synthesis, quantum-chemical characterization, and in vitro cytotoxicity

Stefan Richter^a, Milena R. Kaluđerović^b, Martin Bette^a, Fabian Mohr^c, Christoph Wagner^a, Dušan D. Dimić^d, Goran N. Kaluđerović^{e,*}

- ^a Institut für Chemie Martin-Luther-Universität Halle-Wittenberg Kurt-Mothes-Straße 2, 06120 Halle, Germany
- b Department of Oral, Maxillary, Facial and Reconstructive Plastic Surgery, University Hospital of Leipzig, 04103 Leipzig, Germany
- ^c Anorganische Chemie, Fakultät für Mathematik und Naturwissenschaften, Bergische Universität Wuppertal, 42119 Wuppertal, Germany
- ^d Faculty of Physical Chemistry, University of Belgrade, Studentski Trg 12-16, 11000 Belgrade, Serbia
- e Department of Engineering and Natural Sciences, University of Applied Sciences Merseburg, Eberhard-Leibnitz-Straße 2, 06217 Merseburg, Germany

ARTICLE INFO

Keywords: Platinum(II) complexes PTA DFT NMR Cytotoxic activity QTAIM

ABSTRACT

Acetylplatinum(II) complexes containing the water-soluble phosphine ligands based on PTA (1,3,5-triaza-7-phosphaadamantane) were synthesized and structurally characterized: cis-[Pt(COMe)₂(PTA)₂] (3) and trans-[Pt(COMe)₂(PTA)₂] (3a) was obtained from the methanol solution of 3 and structurally characterized. The compounds were investigated by elemental analysis, IR, multinuclear NMR spectroscopy, and mass spectrometry. X-ray crystallography confirmed the square-planar geometry of complexes 3 and 3a, and their supramolecular architectures were examined using Hirshfeld surface analysis. DFT calculations at the B3LYP/LanL2DZ level provided good agreement with experimental bond lengths and angles. NMR spectra were further supported by GIAO-calculated chemical shifts. Intermolecular and intramolecular interactions were elucidated through QTAIM analysis, revealing partial covalent character of metal-ligand bonds and weak non-covalent stabilizing interactions. Complexes 3 and 4 were tested for their in vitro cytotoxicity against five human cancer cell lines (8505C thyroid cancer, A253 head and neck tumor, A549 lung carcinoma, A2780 ovarian cancer, and DLD-1 colon carcinoma). Complex 3 showed selective activity against lung A549 and ovarian A2780 cell lines, comparable to cisplatin, whereas complex 4 exhibited broader but less selective cytotoxicity. These results suggest that the PTA-based acetylplatinum(II) complexes represent promising candidates for further development of water-soluble antitumor agents.

1. Introduction

Many metal compounds are widely used in medicine as diagnostic and therapeutic agents (e.g., contrast agents, radiopharmaceuticals, antiulcer and antitumor drugs, and others) [1–9]. Platinum compounds, in particular, have been used in medicine since the discovery of the cytotoxic activity of cisplatin, cis-[PtCl₂(NH₃)₂], by Barnett Rosenberg in 1969 [10]. Subsequently, a series of new platinum(II) compounds have been tested, and several of them (carboplatin, oxaliplatin, nedaplatin) are successfully used in medicine as cytotoxic drugs. However, those drugs exhibit poor water solubility. Besides success in the fight against cancer, platinum-based drugs are inducing severe side effects, limiting their application. Because of that, the synthesis of platinum-based compounds with improved biological and physical

properties plays an important role in medicinal chemistry.

While phosphine ligands were historically considered unsuitable for biological systems due to concerns about oxidative sensitivity and reactivity, certain water-soluble cage phosphines, such as 1,3,5-triaza-7-phosphaadamantane (PTA), have proven to overcome these limitations. PTA, in particular, offers excellent air and moisture stability, making it a valuable ligand for designing biologically relevant metal complexes [11, 12]. One approach to obtain water-soluble platinum compounds might be to use water-soluble phosphine ligands like the well-known cage phosphine PTA [11,13]. Its compact, cage-like structure provides notable steric protection to the metal center, which contributes to the overall stability of the complex in aqueous and physiological environments. These characteristics have sparked renewed interest in PTA-based platinum(II) compounds, some of which have shown

E-mail address: goran.kaluderovic@hs-merseburg.de (G.N. Kaluđerović).

^{*} Corresponding author.

promising cytotoxic activity, including against cancer cells that are resistant to classical platinum drugs. In addition to platinum(II), PTA has also been successfully coordinated to copper(I), palladium(II), as well as ruthenium(II), yielding complexes with encouraging biological properties and therapeutic potential [14–16]. The favorable solubility and robust coordination behavior of PTA continue to support its use in the development of next-generation metallodrugs [17].

Platinum(II) complexes incorporating the water-soluble phosphine ligand PTA have attracted increasing attention due to their favorable properties such as air and water stability, strong basicity, and compact steric profile [17-21]. PTA ligands predominantly coordinate through the phosphorus atom, forming well-defined square planar geometries around the platinum(II) center. The coordination chemistry of PTA with platinum enables the formation of cis- and trans-isomers of four-coordinate platinum(II) species, which are not only structurally robust but also synthetically accessible in high yields. The presence of PTA ligands enhances the solubility of such complexes in aqueous media, which is particularly advantageous for catalytic and medicinal applications. In recent years, numerous new transition metal complexes containing the PTA ligand have been prepared, e.g., [Ni(CN)₂(PTA)₃], [PdCl₂(PTA)₂], [PtCl₂(PTA)₂], and [RhCl₂(PTA)₄] [11,21-31]. Most compounds containing PTA or its derivatives show good water solubility, which can be important for their in vivo application as antitumor agents. PTA shows a high solubility in polar protonated solvents. Therefore, the PTA ligand is very interesting for synthesizing new water-soluble cytotoxic drugs.

The aim of this contribution is to prepare acetylplatinum(II) complexes with PTA: cis-[Pt(COMe)₂(PTA)₂] (3), and trans-[Pt(COMe)Cl (PTA)₂] (4). These compounds were characterized by elemental analysis, mass spectrometry, FTIR, and NMR techniques. The molecular structures of 3 and its trans isomer 3a, trans-[Pt(COMe)₂(PTA)₂], were determined by X-ray crystallography, and the stabilization interactions with co-crystallized solvent molecules were assessed by the Hirshfeld surface analysis. Complexes 3 and 4 were designed to explore how variations in ligand environment influence the structure of platinum(II) compounds bearing PTA. Specifically, it is aimed to compare the impact of two acetyl ligands (3) versus one acetyl and one chlorido ligand (4) on the geometric arrangement and biological activity. The incorporation of PTA was motivated by its known kinetic inertness, air/moisture stability, and aqueous solubility, which make it a suitable ligand for biologically oriented platinum(II) chemistry.

The experimental structures were optimized at the B3LYP/6–311++G(d,p)(C,H,N,O,P)/LanL2DZ(Pt) level of theory, and the experimental and theoretical bond lengths and angles were compared. The 1 H and 13 C NMR spectra were predicted and examined with experimental ones. The interactions between the central metal atom and surrounding ligands were investigated by the Quantum Theory of Atoms in Molecules (QTAIM), and the effects of isomerisation and the presence of a chlorine atom were elucidated. The cytotoxic activity of $\bf 3$ and $\bf 4$ was determined toward 518A2, 8505C, A253, MCF-7, and SW480 cell lines.

2. Materials and methods

2.1. General

All reactions were performed under an N_2 atmosphere using standard Schlenk techniques. Solvents were dried using standard procedures (dichloromethane, methanol) and distilled before use. NMR spectra (1 H, 13 C, 31 P) were recorded at 27 °C on Varian Gemini 2000 (200 MHz) and Unity 500 (500 MHz) spectrometers. Chemical shifts are relative to solvent signals (CDCl₃; δ_H 7.24, δ_C 77.0) as internal references. H₃PO₄ (85 %) was used as an external reference for 31 P NMR spectra. Multiplets of higher order are enclosed in inverted commas or designated as multiplet (m); the coupling constants were obtained by simulation using the Perch-NMR software package (Perch Solutions Ltd.) [27]. IR spectra were recorded on a Bruker Tensor 27-IR spectrometer with a Platinum

ATR unit. ESI mass spectra were performed with an LCQ mass spectrometer (Finnigan Mat.) operating in positive ion mode. Microanalyses were performed at the Martin Luther University Halle-Wittenberg, microanalytical laboratory, using a VarioEL elemental analyzer. The complexes $[Pt(COMe)_2(NH_2Bn)_2]$ (1) and $bis[\mu\text{-chlorido}(l\text{-platina-dimethyl-}\beta\text{-diketone})] <math>[Pt_2\{(COMe)_2H\}_2(\mu\text{-Cl})_2]$ (2) were prepared according to literature methods [32,33], whereas all other chemicals were purchased from Aldrich or Fluka and used as obtained.

2.2. Synthesis of compounds

2.2.1. Synthesis of cis- $[Pt(COMe)_2(PTA)_2]$ (3)

To a solution of $[Pt(COMe)_2(NH_2Bn)_2]$ (1) (450 mg, 0.91 mmol) in dichloromethane (30 mL), PTA (290 mg, 1.82 mmol) was added with stirring. After 10 min, the solvent was reduced in vacuum to about 10 mL. Subsequently, diethyl ether (5 mL) was added, and the formed yellow precipitate was filtered off and washed with diethyl ether (3 mL) and dried in a vacuum. NMR spectra are presented in Fig. S1. Yield: 83 % (450 mg). $T_{dec.} = 155 \,^{\circ}\text{C}$. Elem. anal. (found (calc.), %): $C_{16}H_{30}O_{2}N_{6}P_{2}Pt$ (Mr = 595.48), C 32.41 (32.27), H 4.68 (5.08), N 14.19 (14.11). ¹H NMR (200 MHz, CD₃OD): δ 2.03 (s+d, ${}^{3}J_{\text{Pt,H}}=16.9$ Hz, 6H, COCH₃), 4.05 (s, 12H, PCH₂N), 4.52 (s, 12H, NCH₂N). ${}^{13}\text{C}$ NMR (51 MHz, CD₃OD): δ 44.7 (m+dm; calc.: ${}^{3}J_{\text{P,C}}=22.5$ Hz, ${}^{3}J_{\text{P',C}}=1.0$ Hz, ${}^{2}J_{\text{P,P}}=-18.8$ Hz, COCH₃), 52.7 (m; calc.: ${}^{1}J_{P,C} = 15.5 \text{ Hz}$, ${}^{3}J_{P,C} = 2.5 \text{ Hz}$, PCH₂N), 73.1 (s, NCH₂N), 255.8 ('dd'+'dd', ${}^{1}J_{Pt,C} = 915 \text{ Hz}$, CO). ³¹P NMR (81 MHz, CD₃OD): δ –70.3 (s + d, ${}^{1}J_{\text{Pt},P}$ = 1470.0 Hz). ESI-MS: m/z (Int. found/ calc. for [Pt(COMe)₂(PTA)₂Na]⁺, %) 615.14 (0/1), 617.14 (80/82), 618.14 (100/100), 619.14 (79/81), 620.14 (13/15), 621.14 (19/19), 622.14 (4/4), 623.14 (0/0.4). IR: v 2944 (w), 2872 (w), 1636 (s), 1414 (m), 1278 (m), 1238 (s), 971 (s), 806 (m), 570 (m), 256 (m) cm⁻¹. Crystals of 3-MeCN suitable for X-ray diffraction analysis were obtained by crystallization in MeCN at low temperature (-40 °C).

2.2.2. Synthesis of trans-[Pt(COMe)2(PTA)2] (3a)

Upon recrystallization of compound 3 from methanol at room temperature, well-formed crystals of the *trans* isomer (3a) were obtained over 12 days. Compound 3a was isolated in very low yield as single crystals suitable for X-ray diffraction. Due to the limited amount of material, no further characterization was able to be carried out.

2.2.3. Synthesis of trans-[Pt(COMe)Cl(PTA)₂] (4)

2.2.3.1. From the reaction of complex 3 with HCl. To a solution of cis-[Pt (COMe)₂(PTA)₂] (3; 100 mg, 0.17 mmol) in methanol (10 mL), hydrochloric acid (0.50 mmol; 1.7 M) was added dropwise with stirring. After a few minutes, gas development and formation of the precipitate were observed. After stirring the reaction mixture for 24 h at room temperature, a methanolic solution of NaOMe (6 mL, 2.4 mmol; 0.4 M) in an ice bath, at 0 °C, was added dropwise. Then, the reaction mixture was stirred for 10 min, and the precipitate formed was filtered off, washed with a methanolic solution of NaOMe (3 mL; 0.4 M) and methanol (4 mL), and dried in a vacuum. NMR spectra are presented in Fig. S2. Yield: 40 mg (40 %). EA (found. (calc.), %): $C_{14}H_{27}ON_6P_2ClPt$ (Mr = 587.88), C 28.90 (28.60), H 4.16 (4.63), N 13.94 (14.29). ¹H NMR (200 MHz, CDCl₃): δ 2.18 (s+d, ${}^3J_{\text{Pt},H}=12.6$ Hz, 3H, COCH₃), 4.18 (s, 12H, PCH₂N), 4.45 (s, 12H, NCH₂N). 13 C NMR (125 MHz, CDCl₃): δ 48.5 (t, $^{3}J_{P,C} = 9.9$ Hz, COCH₃), 50.2 ('t' + d't', calc.: $^{1}J_{P,C} = 20.8$ Hz, $^{2}J_{Pt,C} =$ 43.9 Hz, PCH₂N), 73.2 (t, ${}^{3}J_{P,C} = 7.4$ Hz, NCH₂N), 212.3 (t, ${}^{2}J_{P,C} = 13.7$ Hz, COCH₃). 31 P NMR (81 MHz, CDCl₃): δ –61.4 (s+d, $^{1}J_{\text{Pt},P}=3036$ Hz). IR: v 3466 (w), 2966 (w), 1636 (s), 1421 (s), 1336 (s), 1228 (m), 1085 (m), 977(s), 885 (s), 799 (s) cm⁻¹.

2.2.3.2. From the reaction of complex 2 with PTA. At -80 °C, to a solution of platina- β -diketone [Pt₂{(COMe)₂H}₂(μ -Cl)₂] (2) (100 mg, 0.16 mmol) in methanol (5 mL), PTA (50 mg, 0.32 mmol) was added with

stirring. After 40 min, the solvent was removed under vacuum, and the solid residue was dissolved in dichloromethane (5 mL). After adding diethyl ether (6 mL), a yellow product precipitated, which was filtered off, washed with diethyl ether (3 mL), and dried in a vacuum. Yield: 100 mg (53 %). ^1H NMR (200 MHz, CDCl₃): δ 2.18 (s, 3H, COCH₃), 4.19 (s, 11H, PCH₂N), 4.45 (s, 12H, NCH₂N). ^{31}P NMR (81 MHz, CDCl₃): δ –61.4 (s + d, $^1J_{\text{PL,P}}$ = 3036 Hz).

2.3. X-ray crystallography

Single crystals of 3·MeCN, obtained by crystallization in MeCN (-40 °C). Suitable crystals for X-ray analysis of 3a·MeOH were formed from the MeOH solution of 3 at room temperature over 12 days. X-ray diffraction measurements were performed on a Stoe-IPDS2T diffractometer at 200(2) K using Mo K α radiation ($\lambda = 0.71073$ Å, graphite monochromator). A summary of the crystallographic data, the data collection parameters, and the refinement parameters is given in Table 1. Multiscan absorption corrections were applied using the SHELXT program package (T_{\min}/T_{\max} 0.26/0.51, **3·MeCN**; 0.12/0.63, 3a·MeOH) [34]. The structures were solved with direct methods using SHELXT and refined using full-matrix least-squares routines against F² with SHELXL. All non-hydrogen atoms were refined with anisotropic displacement parameters. Hydrogen atoms were placed in calculated positions and refined using the riding model with an isotropic displacement parameter of 1.5Ueq of the parent atom for methyl hydrogens and 1.2Ueq for all other hydrogen atoms. CCDC 2465003 and 2465,004 contain the supplementary crystallographic data for compounds 3:MeCN and 3a:MeOH. These data can be obtained free of charge from The Cambridge Crystallographic Data Centre via www.cc dc.cam.ac.uk/data request/cif.

2.4. Hirshfeld surface analysis

The crystallographic structures of *cis* and *trans* isomers of [Pt (COMe)₂(PTA)₂] were examined using Hirshfeld surface analysis. These surfaces were visualized in the CrystalExplorer program [35] starting from the experimental structural files. Hirshfeld surface is presented as a graph connecting two distances, one between two nearest nuclei (de) and the second one connecting nuclei with the external surface (di) [36, 37]. These distances are colored red, white, and blue if the separations

Table 1
Crystal Data and Structure Refinement for 3·MeCN and 3a·MeOH.

	3-MeCN	За-МеОН
Empirical formula	$C_{18}H_{33}N_7O_2P_2Pt$	$C_{18}H_{38}N_6O_4P_2Pt$
Formula weight	636.54	659.57
Crystal system	monoclinic	triclinic
Space group	$P2_1/c$	$P\overline{1}$
a (Å)	11.9392(3)	6.2834(3)
b (Å)	14.8000(4)	10.2552(6)
c (Å)	13.3131(3)	10.5212(6)
α (°)		116.936(4)
β (°)	104.818(2)	100.179(4)
γ (°)		91.285(5)
$V(\mathring{A}^3)$	2274.19(10)	590.83(6)
Z	4	1
$D_{\rm calc}$ (g·cm ⁻³)	1.859	1.854
$\mu(\text{Mo-K}_{\alpha}) \text{ (mm}^{-1})$	6.341	6.110
F(000)	1256	328
θ range (°)	2.75-27.00	2.22-29.67
Reflections collected	18,333	9759
Reflections observed $[I > 2\sigma(I)]$	4665	3177
Independent reflections	$4962 [R_{\rm int} = 0.0192]$	3177 $[R_{int} = 0.0411]$
Data/restrains/parameters	4962/0/274	3177/0/145
Goodness-of-fit on F ²	1.058	1.072
Final <i>R</i> indices $[I > 2\sigma(I)]$	$R_1 = 0.0269$	$R_1 = 0.0229$
	$wR_2 = 0.0677$	$wR_2 = 0.0546$
R indices (all data)	$R_1 = 0.0286$	$R_1 = 0.0185$
	$wR_2 = 0.0688$	$wR_2 = 0.0564$
R indices (all data)	$R_1 = 0.0286$	$R_1 = 0.0185$

between respective nuclei are shorter, equal, or longer than van der Waals separations between atoms. The normalized distances are shown in the range: -0.1660 and 1.4632 for the cis isomer, and -0.5921 and 1.1552 for the trans isomer. The percentages of the most important contacts are discussed in the main text, while the fingerprint plots are given in the Supplementary Information.

2.5. Theoretical structural analysis

The optimization of selected structures was performed in the Gaussian 09 Program package [38]. The crystallographic structures of cis and trans isomers of [Pt(COMe)2(PTA)2] were optimized at B3LYP/6-311++G(d,p)(H,C,N,O,P,Cl)/LanL2DZ(Pt) [39-41] level of theory, which was previously applied for the examination of structural features of other platinum complexes in the references [42,43]. The optimization was done without any geometrical constraints. The applicability of the selected level of theory was shown by comparing the experimental and theoretical bond lengths and angles of the mentioned compounds. Additionally, the structure of complex 4 was optimized at the same level of theory to investigate structural changes that occurred due to the change of one of the ligands. The structures were reoptimized in the solvents that were used for the preparation of NMR spectra (chloroform and methanol) to mimic the experimental conditions by employing the Conductor-Like Polarizable Continuum (CPCM) [44]. The NMR chemical shifts were obtained within the Gauge Independent Atomic Orbital Approach (GIAO) [45,46], relative to TMS, used as the internal standard. The stabilization interactions within structures were identified and quantified using the Quantum Theory of Atoms in Molecules (QTAIM) approach [47,48] in the AIMAll program package. The input files for QTAIM analysis were .wfx files from Gaussian 09.

2.6. In vitro cytotoxic studies

The cell lines: 8505C (thyroid cancer), A253 (head and neck tumor), A549 (lung carcinoma), A2780 (ovarian cancer), and DLD-1 (colon carcinoma) were kindly provided by Dr. Thomas Müller, Department of Hematology/Oncology, Martin-Luther-University of Halle-Wittenberg, Halle (Saale), Germany. Cultures were maintained as monolayers in RPMI 1640 (PAA Laboratories, Pasching, Austria) supplemented with 10 % fetal bovine serum (Biochrom AG, Berlin, Germany) and penicillin/streptomycin (PAA Laboratories) at 37 °C in a humidified atmosphere with 5 % CO₂. Stock solutions of investigated compounds were freshly prepared in dimethylsulfoxide (DMSO, Sigma Aldrich) at a concentration of 20 mM, filtered through a Millipore filter, 0.22 μ m, before use, and immediately diluted in the nutrient medium to various working concentrations. Nutrient medium was RPMI-1640 (PAA Laboratories) supplemented with 10 % fetal bovine serum (Biochrom AG) and penicillin/streptomycin (PAA Laboratories).

The cytotoxic activities of all the compounds were evaluated using the sulforhodamine-B (SRB) (Sigma Aldrich, Germany) microculture colorimetric assay [15]. The cells were treated with serial dilutions of the compounds (0 to 100 μM) for 96 h, and the assay was performed in triplicate. The final concentration of DMSO solvent never exceeded 0.5 %, at which it was non-toxic to the cells. Absorbance was measured at 570 nm using a 96-well plate reader (Tecan Spectra, Crailsheim, Germany). The IC_{50} values were estimated from the semilogarithmic dose-response curves.

3. Results and discussion

3.1. Synthesis and characterization

The new platinum(II) complexes have been synthesized starting from $[Pt(COMe)_2(NH_2Bn)_2]$ (1) or dinuclear platina- β -diketone $[Pt_2\{(COMe)_2H\}_2(\mu\text{-Cl})_2]$ (2) (Scheme 1). Complex 3 expressed good water solubility. 3 reacts with HCl, yielding *trans*-configured

Scheme 1. Synthesis of cis- and trans-configured platinum(II) complexes 3 and 4.

(monoacetyl)platinum(II) complex 4 (Scheme 1). In the reaction of platina- β -diketone **2** with PTA ligand, only *trans*-standing (monoacetyl) platinum(II) complex 4 was available (Scheme 1). The obtained (monoacetyl)platinum(II) complex (4) showed no solubility in water. The IR spectrum of the complex 3 exhibits characteristic absorbance with frequencies from 1600 to 1636 cm⁻¹, corresponding to stretching frequencies of C=O, as described in the literature [49]. However, when recrystallized from methanol at room temperature, well-formed crystals of the trans isomer were obtained in low yields. The absence of any indication of an isomeric mixture in the 31P NMR spectra of solutions of complex 3 (Fig. S3) suggests that the trans isomer is virtually insoluble in methanolic solution and thus precipitates due to its low solubility. Consequently, no conclusions can be drawn regarding the thermodynamic stability of the *cis* versus *trans* isomers. The isomerization appears to proceed at a significant rate only at room temperature, as no formation of the *trans* isomer was observed at –40 °C. Comparable examples in the literature demonstrate that trans-arylplatinum(II) compounds, such as bis(2,6-dinitroaryl)platinum(II) complexes, can undergo isomerization to the corresponding cis isomers upon heating to elevated temperatures (160 °C) [50].

The diacetylplatinum(II) complex **3** and the acetylchloridoplatinum (II) complex **4** theoretically can each exist in *cis* and *trans* configurations. The platinum isotope 198 Pt (33.3 %, $I=\frac{1}{2}$) serves as an ideal probe for configuration determination via NMR spectroscopy. The 195 Pt satellites observed in the 31 P{ 1 H} NMR spectra provide insights into the nature of the donor atoms *trans* to the phosphorus ligands (Figs. S1 and S2), and thereby the geometry of the complexes.

The one-bond coupling constant ${}^1J_{\text{Pt,P}}$ is sensitive to the electronic influence of the ligand positioned *trans* to the phosphorus atom (*trans* influence). A high ${}^{11}J_{\text{Pt,P}}$ value indicates a low *trans* influence and vice versa, due to the dominance of the Fermi contact mechanism [51,52]. For complex 3, a square planar *bis*(PTA)diacetylplatinum(II) complex, a relatively small ${}^{1}J_{\text{Pt,P}}$ coupling constant (1470 Hz) is observed, indicative of a strong *trans* influence from the acetyl ligands and a correspondingly high *s*-character in the Pt–C bonds [53,54]. This is consistent with literature data for related *cis*-[Pt(COMe)₂(PPh₃)₂] complexes (${}^{1}J_{\text{Pt,P}}$ = 1591 Hz), supporting the *cis* configuration of the cage phosphane

ligands in complex 3.

In contrast, complex **4**, a *bis*(PTA)acetylchloridoplatinum(II) complex, exhibits a significantly larger $^1J_{Pt,P}$ coupling constant (3036 Hz), thus 1566 Hz higher than that of complex **3**. This increase reflects the much lower *trans* influence of the chlorido ligand, which enhances the *s*-character of the Pt–P bonds. These values are in line with those of structurally related *trans*-[Pt(COMe)Cl(PPh₃)₂] ($^1J_{Pt,P} = 3036$ Hz) and *trans*-organoplatinum(II) complexes bearing cage phosphane ligands [31,55], thereby confirming the *trans* arrangement of the phosphorus donors in complex **4**.

One resonance signal for the upper and the lower rim of PTA can be observed in the $^1\mathrm{H}$ and $^{13}\mathrm{C}$ NMR spectra of complex 3 (Fig. S1). All protons of the upper rim were found in the $^1\mathrm{H}$ NMR spectrum as a complicated AA'BB'MM'X spin system. Four protons represented the AA'BB' part of the upper rim; the X part results from the $^{31}\mathrm{P}$ nucleus. The other two protons of the methylene group of the upper rim are enantiotopic to each other and observed only as one signal, which appears as a doublet because of a coupling over two bonds to the $^{31}\mathrm{P}$ nucleus. These two protons represented the MM' part of the observed spin system. The two methylene groups of the lower rim are observed as two isolated AB spin systems, with a hydrogen-hydrogen coupling over two bonds.

In all complexes in the 13 C NMR spectra, the methyl carbon atoms from acetyl ligands showed a complicated signal pattern, the result of an ABM-spin system (A, $B = ^{31}$ P, $M = ^{13}$ C) and a satellite spectra (ABMX-spin system; $X = ^{195}$ Pt). Using Perch for spectral analyses, the ABX-spin system was assigned for the complex 3. In Fig. 1. a, the measured and calculated 13 C NMR spectrum of complex 3 is shown.

The carbonyl carbon atoms of the acetyl groups of complex **3** appeared in 13 C NMR spectra as multiplets due to ABMX spin systems (A, $B = ^{31}$ P, $M = ^{13}$ C, $X = ^{195}$ Pt, Fig. 1. b). Only in the case of complex **3** was it possible to determine the $^{1}J_{Pt,C}$ coupling constant (915 Hz). Compared with the literature values in this case, $^{1}J_{Pt,C}$ indicates a *cis*-configured platinum(II) complex. Also, the $^{2}J_{P,P}$ in value of -18.8 Hz found in the 13 C NMR spectrum of complex **3** shows the *cis*-configuration.

In contrast to *cis*-diacetyl-platinum(II) complexes **3**, the *trans*-(monoacetyl)platinum(II) complex **4** shows in the ¹³C NMR spectrum a triplet for the carbonyl carbon atom from the acetyl group. This observation

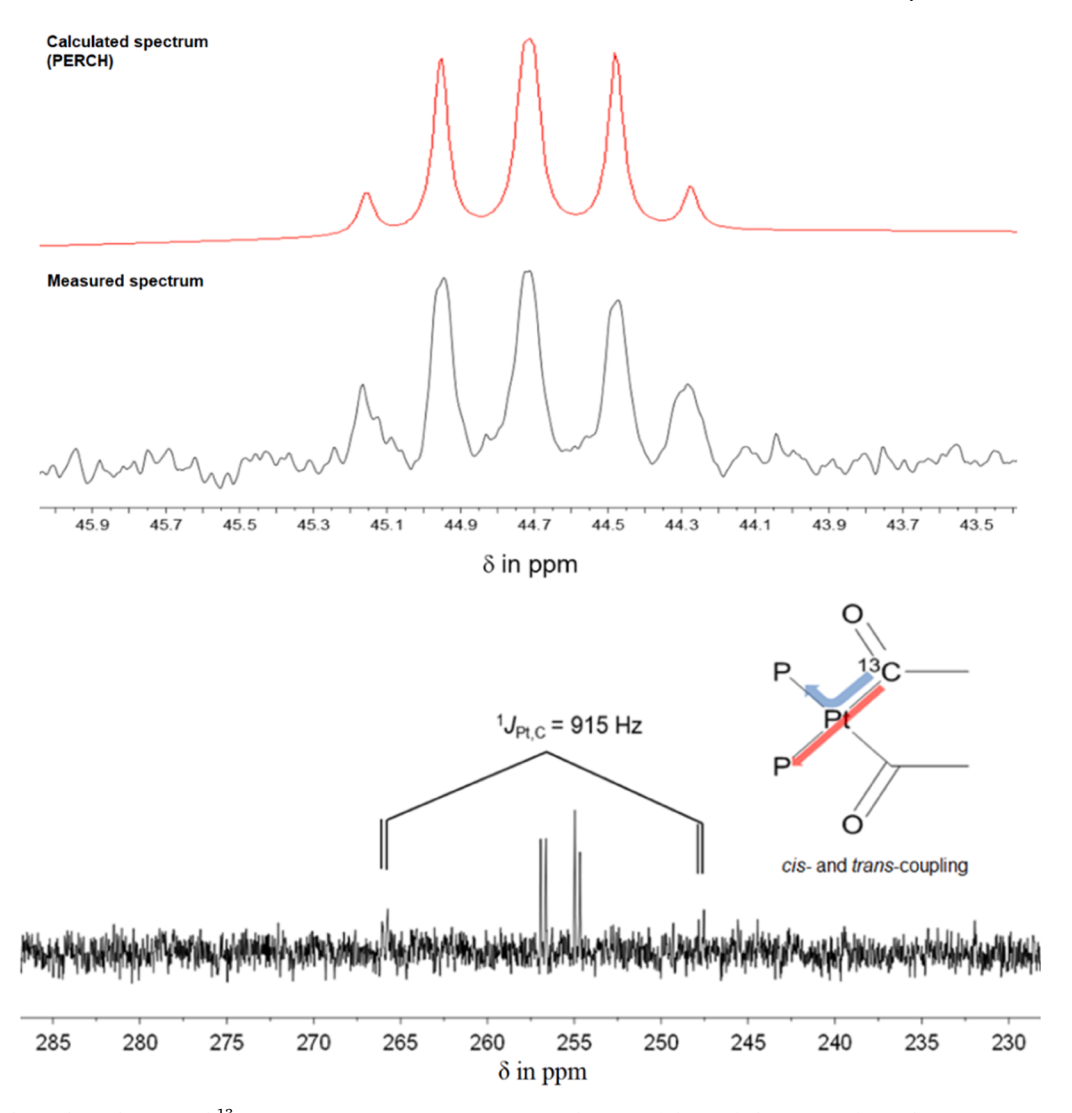


Fig. 1. a) Calculated (Perch) and measured 13 C NMR spectrum (51 MHz, CD₃OD) in the area of the methyl-C-atoms of complex *cis*-[Pt(COMe)₂(PTA)₂] 3; b) 13 C-carbon atom resonances of 3 (CD₃OD, 51 MHz).

suggests the similarity of both phosphorus atoms and thus the *trans*-configuration of complex 4.

3.2. Thermogravimetric analysis

To gain insight into the thermal stability and decomposition pathways, thermogravimetric analyses (TGA, DTG, and DSC) were conducted for complexes 3 and 4 (Figs. S4 and S5). These measurements are relevant for understanding the physicochemical properties of the complexes, which can affect their behavior during storage, processing, or formulation. For complex 3, a two-step thermal decomposition was observed between 160 $^{\circ}\text{C}$ and 320 $^{\circ}\text{C}$ (Fig. S4). The corresponding DSC curve shows that both decomposition events are exothermic. The total mass loss observed was 51.8 %, indicating that complete decomposition to elemental platinum is not achieved even at 1000 °C (theoretical Pt content: 32.8 %). Complex 4 exhibited a comparable thermal profile (Fig. S5). The first mass loss (6.6 %) occurred at approximately 250 °C, which corresponds to the loss of one acetyl group. A second, more pronounced mass loss was observed above 350 $^{\circ}$ C. Both steps were also exothermic. The total mass loss of 56.5 % suggests, similarly to complex 3, incomplete decomposition to metallic platinum at 1000 $^{\circ}$ C. These thermal profiles support the relatively high thermal robustness of both complexes and provide complementary data to their chemical and biological properties.

3.3. Structural characterization

The configuration of the diacetylplatinum(II) complex **3** was unambiguously confirmed, and it crystallizes from acetonitrile in its *cis* form. Complex **3** (Fig. 2. a) crystallized as an acetonitrile adduct in the monoclinic space group $P2_1/c$. The complex **3a** crystallized in the triclinic space group $P\overline{1}$ (Fig. 2. b).

The coordination sphere around the platinum atom is almost square planar (sum of the angles: 359.7°). The acetyl ligands are found in a *trans* arrangement positioned nearly vertical to the PtP1P2C1C3 plane with the inter plane angles of $85.9(2)^{\circ}$ (O1,C1,C2/Pt,P1,P2,C1,C3) and $78.7(1)^{\circ}$ (O2,C3,C4/Pt,P1,P2,C1,C3). The voluminous PTA ligand requires relatively much space, thus deviating from the P1–Pt–P2 angle (99.48 (3)°). In crystals of $3\cdot$ MeCN, no intermolecular distances between 3 and solvent molecules were observed. The shortest atomic distance between nonproton atoms is 3.518(5) Å (O2 $^{\circ\circ}$ CH₃CN). The molecular structure of 3 is shown in Fig. 2. and selected bond distances and angles are collected in Table 2.

In the structure of $3a\cdot MeOH$, similarly to the structure of $3\cdot MeCN$, the platinum atom is square planar coordinated (sum of angles: 360°). The τ_4 values [56] of 0.14 for 3 and 0.00 for 3a further confirm a square-planar coordination geometry. The Pt–P distances of 3a (2.2765 (7) Å) are in comparison to 3 shorter (2.3008(9) and 2.2981(9) Å), which can be attributed to the larger *trans* influence of the acetyl ligands

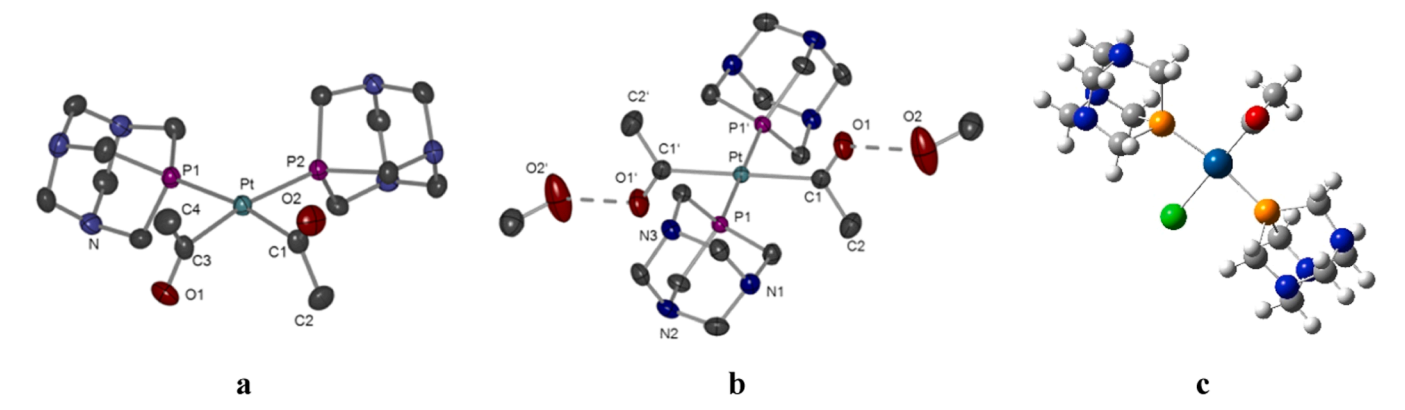


Fig. 2. a) Molecular structure of *cis*-[Pt(COMe)₂(PTA)₂] (3) in crystals of 3·MeCN; b) Structure of *trans*-[Pt(COMe)₂(PTA)₂]·MeOH (3a·MeOH) (The thermal ellipsoids are drawn at a 30 % probability level. Hydrogen atoms are omitted for clarity); c) optimized structure of *trans*-[Pt(COMe)Cl(PTA)₂] (4).

Table 2 Selected bond distances (in Å) and angles (in $^{\circ}$) of cis-[Pt(COMe)₂(PTA)₂] (3) and trans-[Pt(COMe)₂(PTA)₂] (3a) in crystals of 3-MeCN and 3a-MeOH, respectively.

	3	3a
Pt-P1	2.2981(9)	2.2765(7)
Pt-P2	2.3088(9)	
Pt-C1	2.058(4)	2.099(3)
Pt-C3	2.063(4)	
P1-Pt-P2	99.48(3)	180.00(3)
P1-Pt-C1	88.55(11)	88.39(8)
P2-Pt-C3	89.38(10)	
C1-Pt-C3	82.27(15)	
P1-Pt-C3	170.05(10)	91.61(8)
P2-Pt-C1	170.70(11)	

[57–59]. Analogously to **3·MeCN**, the acetyl ligands exhibited transoid with a nearly vertical position to the PtP1P1'C1C1' plane with the inter-plane angle of 84.8(1) (O1,C1,C2/Pt,C1,C1',P1,P1').

Contrary to **3·MeCN**, hydrogen bonds were found in the crystals of **3a·MeOH**, between **3a** and solvent molecules (Fig. 2. b). Namely, a medium-strong hydrogen bond between O1 and O2 atoms (2.790(3) Å) is found [60]. The rest of the bond lenghts and angles are presented in Tables S1-S4.

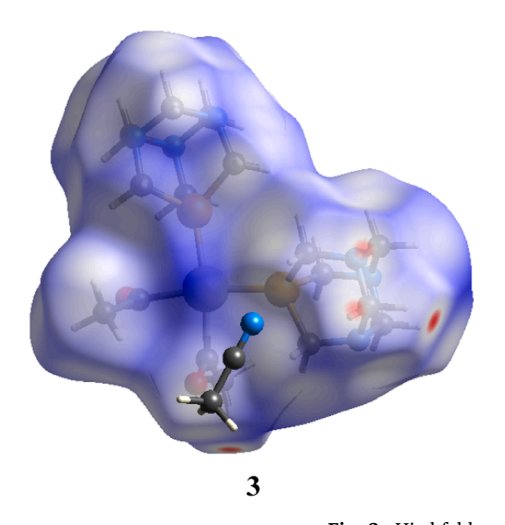
3.4. Hirshfeld analysis of crystal structures

Two crystallographic structures were subjected to the Hirshfeld

surface analysis to examine intramolecular interactions contributing to the system's stability. These surfaces are depicted in Fig. 3. The fingerprint plots of the most numerous contacts are shown in Figs. S6 and S7.

Due to the specific geometry of the *cis*-complex, the interactions involving Pt(II) ions were not observed. The most numerous contacts are denoted as H•••H, with a relative percentage of 68.6 %. These interactions include hydrogen atoms of acetyl groups and the PTA ligand, as these atoms are positioned at the outskirts of the ligands. Nitrogen atoms in the PTA ligand also lead to a large number of hydrogen bonds between nitrogen and hydrogen atoms (N•••H, 16.8 %). The oxygen atoms of acetyl groups interact with neighbouring hydrogen atoms through O•••H interactions (12 %). These interactions are weak, as the hydrogen atoms are not attached directly to the electronegative atoms. Weak carbon-hydrogen bonds are also present in the structure, with a low relative percentage (1.8 %). The carbon atoms also interact with electronegative atoms, oxygen, and nitrogen, through C•••O (0.1 %) and C•••N (0.5 %). A higher percentage of the latter interactions result from the acetonitrile presence in the crystallographic structure.

The relative position of ligands in the structure of **3a•MeOH** induces several changes in the contribution of various contacts. The most important difference is the presence of interactions involving the central metal ion. In this case, Pt(II) interacts with the hydrogen atoms of the PTA ligands, as depicted in Fig. 4. These interactions have a length of 3.06 Å. The contribution of Pt•••H interactions is 0.9 %. The most numerous contacts are again H•••H, and their percentage is almost the same as in **3•MeCN** (68.9 %). The contribution of N•••H contacts is lowered to 12.5 %, while that of O•••H is increased to 16.9 %. The



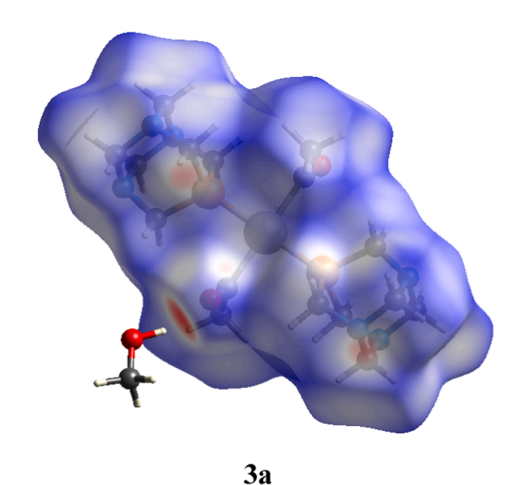


Fig. 3. Hirshfeld surfaces of $\bf 3$ and $\bf 3a$ complexes.

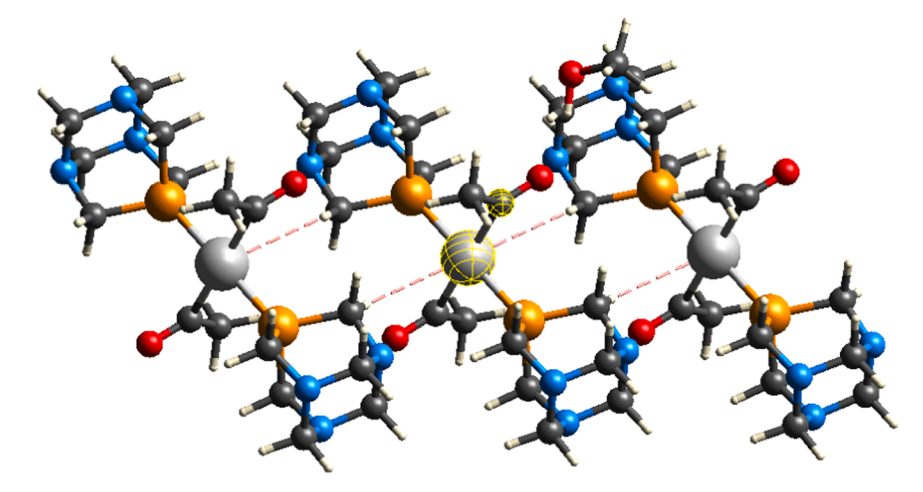


Fig. 4. Representation of Pt •• • H contacts in the structure of 3a.

increase in O•••H contacts is due to the methanol molecules, as a cocrystallized solvent. Therefore, it can be concluded that the orientation of ligands around the central metal ion and the presence of solvents are the main factors influencing the contributions of different interactions in the examined structures. The strength of these interactions is investigated in more detail in the following section.

3.5. DFT structure optimization of complexes 3 and 3a

The optimization of crystallographic structures was performed as previously explained, and the most stable configurations of **3**, **3a•MeOH**, and 4 are presented in Fig. 2. Ongagna and coworkers applied the same level of theory for the DFT assignment of Pt complexes with bis-(N-heterocyclic carbene) ligands [61]. The spectroscopic and structural features of the planar platinum(II) complex with asymmetrically substituted 5-methyl-5'-carbomethoxy-2,2'-bipyridine were also investigated at this level of theory [62]. The experimental and theoretical bond lenghts and angles were compared by calculating the correlation coefficient (R) and the mean absolute error (MAE). The second parameter is the average value of the absolute difference between two data sets. The crystallographic and optimized bond lengths and angles are listed in the Supplementary Information as Tables S1-S4.

The correlation coefficient and MAE for the bond lenghts 3 are 0.998 and 0.019 Å (Table S1). Similar results were found when angles were examined (R=0.993, MAE = 1.11° , Table S2). However, it should be mentioned that the structure of PTA ligands does not allow significant movement of the atoms due to the large number of bonds. The structure of ${\bf 3a\bullet MeOH}$ contains a higher degree of symmetry, as explained in the experimental section. The statistical parameters, R and MAE, in the case of the bond lengths in ${\bf 3a\bullet MeOH}$ are 0.998 and 0.020 Å. As shown in Table S4, the correlation coefficient (0.996) and MAE (1.25°) for angles in the same structure are similar to the values calculated for the 3 structure. These results also prove that the selected theory level is appropriate for describing the two newly obtained structures.

The structure of complex **4** was optimized at the same level of theory, although the crystallographic structure was not obtained. The bond lengths Pt-P are 2.336 Å, almost the same as in the structure of **3a**. This result aligns with the assumption that the bond lengths are not primarily dependent on the other substituents. The Pt-C is slightly shorter (2.020 Å) due to the delocalization within the acetyl group, while the C=O bond is 1.211 Å. The longest ligand-metal bond was found in the case of the Pt-CI bond (2.546 Å). The change in ligands between **3a** and **4** induces additional changes in the values of angles. The value of the P-Pt-P angle is lowered to 170.9° The angles C-Pt-C are around 93° , only 1.5° higher than in **3a**. The angle enclosed by the carbonyl group and Pt(II) is the same as in the optimized structure of **3a**. The

experimental and theoretical NMR spectra of complexes ${\bf 3}$ and ${\bf 4}$ are compared in the following section.

3.6. Comparison of experimental and theoretical NMR spectra

The comparison between experimental and theoretical NMR spectra is crucial for verifying the applicability of the selected theoretical level and the structural characteristics of complexes 3 and 4, particularly because the crystallographic structure of the latter was not obtained. The GIAO method was employed to calculate the chemical shifts of the structures reoptimized in the solvents where the experimental spectra were recorded. The theoretical values of $^1\mathrm{H}$ NMR chemical shifts are presented in Table 3 as calculated through this procedure. Conversely, the $^{13}\mathrm{C}$ NMR chemical shift values were overestimated, especially for the carbonyl carbon atoms, since the explicit solvent effects were not considered in the solvent model used. Therefore, the correction coefficients of 0.92 (3) and 0.85 (4) account for the specific solvent-solute interactions in solution and the effects of local vibrations and rotations of particular groups.

The newly obtained complexes are characterized by only three different proton positions in NMR spectra, and these values exhibit a high resemblance, as anticipated from the structural considerations. The lowest chemical shifts were found for methyl protons at positions 2.03 (3) and 2.18 ppm (4). The calculated values are 2.03 and 2.08 ppm. The protons attached to carbon atoms between nitrogen and phosphorus display higher chemical shift values of 4.05 (3) and 4.18 ppm (4). The differences between experimental and calculated chemical shift values are 0.07 (3) and 0.21 (4). Due to their electronegativity, the hydrogen atoms positioned between two nitrogen atoms are characterized by the highest chemical shift values, around 4.50 ppm. These values are also well reproduced in the optimized structures.

Table 3 Experimental and theoretical (at the B3LYP/6–311++G(d,p)(C,H,N,O,P)/ LanL2DZ(Pt) level of theory) 1 H and 13 C NMR chemical shifts (in ppm) of complexes **3** and **4**.

Atoms	3		4		
	Experimental	Theoretical	Experimental	Theoretical	
COCH ₃	2.03	2.03	2.18	2.08	
PCH_2N	4.05	3.98	4.18	3.97	
NCH_2N	4.52	4.52	4.45	4.52	
CO C H ₃	44.7	40.2	48.5	38.2	
PCH_2N	52.7	55.4	50.2	50.3	
NCH_2N	73.1	72.5	73.2	66.6	
C =OCH $_3$	255.8	256.2	212.3	216.9	

As previously discussed, the ¹³C NMR chemical shifts were overestimated, and the corrected values are used for comparison. The methyl group carbon atoms exhibit characteristic peaks at 44.7/40.2 (3) and 48.5/38.2 ppm (4). The positioning of the other two types of carbon atoms depends on the presence of electronegative atoms. The carbon atoms situated between two nitrogen atoms are identified through peaks at 73.1 and 73.2 ppm in the experimental spectra and at 72.5 and 66.6 ppm in the theoretical spectra of 3 and 4, respectively. The most significant influence of the correction coefficient value was noted for the carbonyl group, as these atoms are affected by the specific interactions formed with methanol/chloroform. Nevertheless, the corrected values are similar to the experimental ones. This analysis aligns with comparing crystallographic and optimized structures, indicating that the theoretical structures can be examined further.

3.7. QTAIM analysis of complexes 3, 3a, and 4

The interactions between central metal ions and donor atoms were investigated using QTAIM analysis Fig. 5), a method well-suited for characterizing coordination environments and calculating metal–ligand interaction energies in platinum complexes [63–65]. For selected interactions, several parameters at the Bond Critical Points (BCPs) were determined: electron density ($\rho(r)$), Laplacian of the electron density ($\nabla^2 \rho(r)$), Lagrangian kinetic energy density (G(r)), potential energy density (G(r)), total electron energy density (G(r)), and the interatomic bond energy (G(r)) and G(r) based on the electron density values at BCPs, Bader and Essen categorized interactions into two types: shared interactions (covalent bonds) with electron density greater than 0.1 a.u., and closed-shell interactions such as hydrogen bonds, ionic bonds, and van der Waals forces, typically with electron density around 0.01 a.u [66,67]. A more detailed classification was later introduced by Bianchi and colleagues, using the ratio of G(r) to V(r) as a

criterion. Covalent interactions correspond to -G(r)/V(r) values below 1, the intermediate (transit) region includes interactions with partial covalent character and values between 1 and 2, while ionic interactions exhibit values exceeding 2 [68]. The nature of an interaction can also be inferred by examining the total electron energy density; a negative value of this parameter suggests covalent character. Interatomic interaction energies were calculated based on potential energy density, following the approach proposed by Espinosa [69]. The QTAIM parameters of complexes 3, 3a, and 4 are presented in Table 4. It should be emphasized that, due to the symmetry of the compounds, only one bond of the same type is shown.

In the structure of 3, the highest electron density and Laplacian value were found for the Pt-C bond, measuring 0.130 and 0.185 a.u., respectively. This bond exhibits a partial covalent character as determined by the large negative value of the total electron density (-138.9) $kJ \text{ mol}^{-1}$) and the -G(r)/V(r) value being lower than 1 [70]. The interatomic bond energy is $-199.4 \text{ kJ mol}^{-1}$. The interaction with phosphorus atoms shows similar characteristics, with $H(r) = -72.6 \text{ kJ mol}^{-1}$ and -G (r)/V(r) = 0.7, although the energy of interaction is lower at -120.1 kJ mol⁻¹. Small values of electron densities, positive values of Laplacian, and negative values of H(r), suggesting partial covalent character [71], were also observed in other platinum complexes [61]. The structure is additionally stabilized by a weak hydrogen bond between the carbonyl oxygen and the hydrogen atom of the PTA ligand. This interaction has a positive H(r) value and a -G(r)/V(r) ratio higher than 1. The energy of this interaction is -7.0 kJ mol^{-1} . The electron density value (0.009 a.u.) of this interaction falls within the range proposed by Popelier for hydrogen-bonded systems [72]. Another weak interaction occurs between two PTA ligands, with an energy of only -3.1 kJ mol⁻¹. However, this demonstrates that the relative distribution of ligands around the central metal ion is responsible for these interactions.

When ligands are in a trans position (3a), the characteristics of the

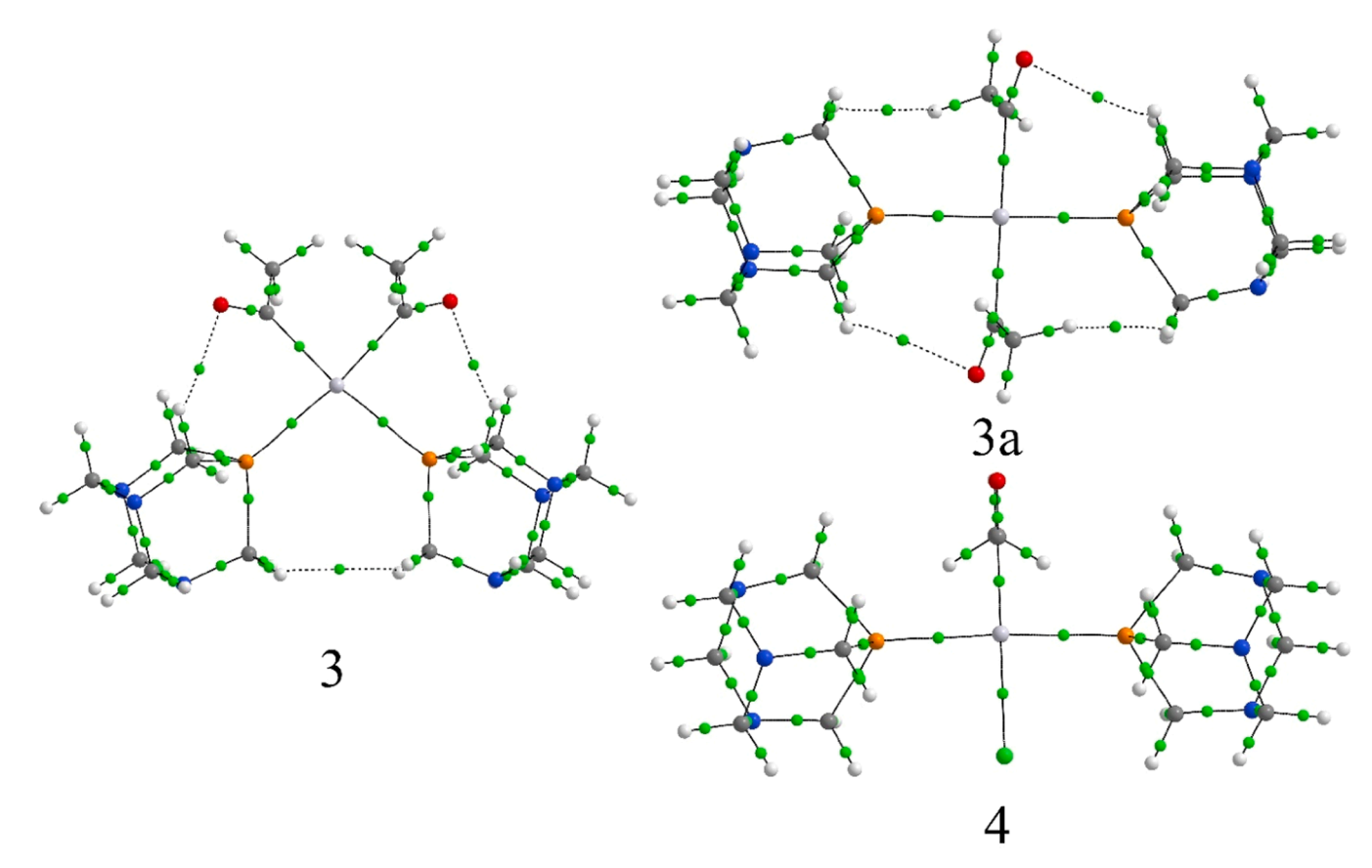


Fig. 5. The BCPs (green spheres) in complexes 3, 3a, and 4.

Table 4
The calculated Bond Critical Points (BCP) properties at the DFT/B3LYP-D3BJ/6-311+G(d,p)(H,C,N,O,P,Cl)/LanL2DZ(Pt) level of theory of complexes 3, 3a, and 4.

Bond	ρ(r) [a.u.]	$ abla^2 \rho(\mathbf{r}) \text{ [a.u.]}$	G(r) [kJ mol ⁻¹]	V(r) [kJ mol ⁻¹]	H(r) [kJ mol ⁻¹]	-G(r)/V(r)	E _{bond} [kJ mol ⁻¹]
3							
Pt-P1	0.083	0.145	167.6	-240.1	-72.6	0.7	-120.1
Pt-C1	0.130	0.185	259.9	-398.8	-138.9	0.7	-199.4
C=O•••HCH	0.009	0.028	16.2	-13.9	2.3	1.2	-7.0
НСН●●●НСН	0.005	0.016	8.2	-6.1	2.1	1.3	-3.1
3a							
Pt-P1	0.100	0.146	196.2	-296.5	-100.3	0.7	-148.2
Pt-C1	0.115	0.199	242.7	-354.7	-112.0	0.7	-177.4
$C = O \bullet \bullet \bullet HCH$	0.004	0.015	8.5	-7.0	1.6	1.2	-3.5
HCH●●●HCH	0.005	0.016	8.8	-7.1	1.7	1.2	-3.6
4							
Pt-P1	0.099	0.139	189.4	-287.9	-98.5	0.7	-144.0
Pt-C	0.145	0.172	281.0	-450.1	-169.1	0.6	-225.1
Pt-Cl	0.057	0.159	135.1	-165.7	-30.6	0.8	-82.8

Pt–P and Pt–C bonds are similar. The strongest interaction remains Pt–C, with electron density and Laplacian values of 0.115 and 0.199 a. u., respectively. The H(r) and -G(r)/V(r) for this bond are $-112.0\,\rm kJ$ mol 1 and 0.7, which is lower than in the structure of 3. The total electron energy and interaction energy of Pt–P are -100.3 and $-148.2\,\rm kJ$ mol $^{-1}$, indicating that these bonds are stronger than in the previous complex. The interactions between the carbonyl oxygen and hydrogen atoms of PTA are weaker, with an interaction energy of $-3.5\,\rm kJ$ mol $^{-1}$. There is also an additional interaction between the methyl group of the acetyl ligand and the hydrogen atoms of PTA, with a comparable interaction energy of $-3.6\,\rm kJ$ mol $^{-1}$.

The connection between the computational results and experimental behavior provides insight into the observed stability and reactivity of the studied complexes. The QTAIM analysis revealed stronger Pt–C and Pt–P interactions in complex 3 compared to its *trans* isomer 3a, aligning with the experimental observation that complex 3 is the major product under standard conditions. Furthermore, the presence of weak stabilizing hydrogen bonds in the *cis*-isomer supports its increased thermodynamic stability, which is corroborated by the calculated energy difference of 26.7 kJ mol⁻¹, favoring the *cis* form. The lower solubility of the *trans* isomer and its slow formation at room temperature are consistent with its reduced stabilization from weak intramolecular interactions. The importance of these interactions for the stability of platinum(II) complexes is outlined in the paper by Szmigiel-Bakalarz and coworkers [73].

Once the acetyl group is exchanged for a chlorine atom in the structure of complex 4, the strength of the remaining Pt-C bond increases, as verified by the electron density (0.145 a.u.), Laplacian (0.172 a.u.), total electron energy (-169.1 kJ mol⁻¹), and interatomic bond energy (-225.1 kJ mol⁻¹). The parameters of the Pt-P bond remain similar to those of the 3a complex. The bond between platinum(II) and chlorine is the weakest of these bonds, with an electron density of 0.057 a.u. and a Laplacian of 0.159 a.u. This bond still possesses partial covalent character, indicated by a negative H(r) value of -30.6 kJ mol⁻¹ and a -G(r)/V(r) value of 0.8. Lu and coworkers also described Pt-Cl as interactions with some degree of covalent character; the H(r) values were negative [74]. The interatomic bond energy measures -82.8 kJ mol⁻¹. Despite the absence of additional weak stabilizing interactions, complex 4 exhibits higher thermal stability, as evidenced by its decomposition onset at \sim 250 °C compared to \sim 160 °C for complex 3. This trend is consistent with the presented QTAIM analysis, which reveals stronger Pt-C and Pt-P interactions in complex 4.

3.8. Cytotoxicity studies

The new platinum(II) complexes, **3** and **4**, were tested against the five human cancer cell lines: 8505C (thyroid cancer), A253 (head and neck tumor), A549 (lung carcinoma), A2780 (ovarian cancer), and DLD-1 (colon carcinoma) (Table 5). For comparison, the cytotoxicity of cisplatin is included.

Table 5 $IC_{50} [\mu M]^a$ values of complexes **3** and **4** against 8505C (thyroid), A253 (head and neck), A549 (lung), A2780 (ovarian), and DLD-1 (colon carcinoma)^a.

	IC_{50} [μM] \pm SD				
compound	8505C	A253	A549	A2780	DLD-1
3	85.97 ±1.51	3.11±0.25	1.75±0.13	2.87±0.04	>150
4	32.37 ± 0.78	$20.02 \\ \pm 0.81$	51.64 ±3.42	23.79 ± 1.92	>150
cisplatin	5.02 ± 0.23	$\begin{array}{c} \textbf{0.81} \pm\\ \textbf{0.20} \end{array}$	$1.51 {\pm} 0.02$	$0.55{\pm}0.03$	$\begin{array}{c} 5.14 \\ \pm 0.12 \end{array}$

 $^{^{\}mathrm{a}}$ Average value \pm Standard deviation from three experiments.

Complex **3**, a water-soluble *cis*-[Pt(COMe)₂(PTA)₂] species, exhibited notable selectivity and high potency against A549 and A2780 cells, with IC₅₀ values of 1.75 and 2.87 μ M, respectively, comparable to cisplatin. However, it was significantly less active toward 8505C and showed no measurable effect on DLD-1 cells (IC₅₀ > 150 μ M), indicating a degree of cell-line specificity that may result from selective uptake or interaction with intracellular targets. It should be noted that the cytotoxicity results reflect the activity of the pure *cis*-isomer, as the freshly prepared solutions were used. The isomerization to the *trans* form occurs slowly over days and was not observed under the conditions relevant for biological testing.

In contrast, complex **4**, trans-[Pt(COMe)Cl(PTA)₂], bearing a chlorido in place of one acetyl ligand, demonstrated a broader but less potent cytotoxic profile. It was more active than complex **3** against 8505C (32.37 μ M vs. 85.97 μ M) and maintained activity against other lines but with reduced potency against A549 and A2780 (IC₅₀ = 51.64 and 23.79 μ M, respectively). These results suggest that substitution of the acetyl group with chlorido ligand affects biological activity, possibly by altering the compound's reactivity or affinity for cellular targets.

The differences in biological activity can be rationalized based on the structural and electronic features of the complexes. QTAIM analysis reveals that complex 3 possesses moderately strong Pt–C and Pt–P bonds ($E_{bond}=-199.4$ and -120.1 kJ mol $^{-1}$) and additional weak hydrogen bonding interactions that may promote a more rigid and defined coordination environment, favoring specific biomolecular recognition. The increased polarity and aqueous solubility of complex 3 could also facilitate uptake in certain cell types. Conversely, complex 4, although electronically stabilized by stronger Pt–C (-225.1 kJ mol $^{-1}$) and Pt–P (-144.0 kJ mol $^{-1}$) interactions, contains a weaker Pt–Cl bond (-82.8 kJ mol $^{-1}$), which may promote ligand exchange or off-target reactivity, resulting in broader but less selective cytotoxicity.

Overall, these findings underscore the critical role of ligand environment in modulating the reactivity and selectivity of platinum(II)–PTA complexes. Fine-tuning coligands, such as replacing acetyl with chlorido, significantly impacts cytotoxic performance and highlights the

potential for structure-based optimization in anticancer drug design.

4. Conclusion

Three novel acetylplatinum(II) complexes containing PTA-based ligands were synthesized and structurally characterized using spectroscopic, crystallographic, and theoretical methods. The square-planar coordination geometry of the platinum(II) centers in *cis*-[Pt (COMe)₂(PTA)₂] (3) and *trans*-[Pt(COMe)₂(PTA)₂] (3a) was confirmed by single-crystal X-ray diffraction. Structural differences between the *cis* and *trans* isomers were observed, particularly in hydrogen bonding and ligand arrangement. Hirshfeld surface analysis revealed variations in intermolecular contacts depending on the molecular geometry and the presence of solvent molecules.

Geometries were optimized using DFT at the B3LYP-D3BJ/6–311+G (d,p)(H,C,N,O,P,Cl)/LanL2DZ(Pt) level, yielding good agreement with experimental bond lengths and angles. Theoretical and experimental NMR chemical shifts were compared employing the GIAO method, with the $^1\mathrm{H}$ NMR resonances demonstrating excellent consistency. QTAIM analysis was conducted to examine bonding interactions, confirming the partial covalent nature of Pt–C and Pt–P bonds while identifying weak stabilizing interactions between ligands and co-crystallized solvents.

The cytotoxic activities of complexes 3 and 4 were evaluated against five human cancer cell lines. Complex 3 showed selective activity toward A549 and A2780 cells, with IC50 values comparable to cisplatin, while complex 4 exhibited broader but less selective cytotoxicity. The PTA ligand alone was inactive under the tested conditions. These results suggest that the structural and electronic features of the complexes strongly influence their biological activity.

Overall, integrating synthetic, structural, computational, and biological studies has provided a comprehensive understanding of the behavior of PTA-based platinum(II) complexes, highlighting their potential as water-soluble antitumor agents.

CRediT authorship contribution statement

Stefan Richter: Investigation. Milena R. Kaluđerović: Investigation. Martin Bette: Investigation. Fabian Mohr: Conceptualization. Christoph Wagner: Investigation. Dušan D. Dimić: Investigation. Goran N. Kaluđerović: Investigation.

Declaration of competing interest

The authors declare that they have no known competing financial interests or personal relationships that could have appeared to influence the work reported in this paper.

Acknowledgments

The authors acknowledge the financial support of the Ministry of Science, Technological Development and Innovation of the Republic of Serbia (Nos. 451–03–137/2025–03/200146 and 451–03–136/2025–03/200146) and by the German Academic Exchange Service (DAAD HAW EURABridge Projekt-ID: 57656312). We would like to thank Prof. Dr. Dirk Steinborn (Martin Luther University Halle Wittenberg, Germany) for his great help related to this project.

Supplementary materials

Supplementary material associated with this article can be found, in the online version, at doi:10.1016/j.molstruc.2025.143677.

Data availability

Data will be made available on request.

References

- [1] G. Angelovski, What we can really do with bioresponsive MRI contrast agents, Angew. Chem. Int. Ed. 55 (2016) 7038–7046, https://doi.org/10.1002/ anie.201510956.
- [2] E.M. Gale, P. Caravan, A.G. Rao, R.J. McDonald, M. Winfeld, R.J. Fleck, M.S. Gee, Gadolinium-based contrast agents in pediatric magnetic resonance imaging, Pediatr. Radiol. 47 (2017) 507–521, https://doi.org/10.1007/s00247-017-3806-0.
- [3] D. Papagiannopoulou, Technetium-99m radiochemistry for pharmaceutical applications, J. Labelled Comp. Radiopharm.60 (2017) 502–520, https://doi.org/ 10.1002/jlcr.3531.
- [4] A. Lanas, F.K.L. Chan, Peptic ulcer disease, The Lancet 390 (2017) 613–624, https://doi.org/10.1016/S0140-6736(16)32404-7.
- [5] C. Rancoule, J.-B. Guy, A. Vallard, M.B. Mrad, A. Rehailia, N. Magné, Les 50 ans du cisplatine, Bull. Cancer 104 (2017) 167–176, https://doi.org/10.1016/j.bulcan.2016.11.011.
- [6] G.N. Kaluđerović, R. Paschke, Anticancer metallotherapeutics in preclinical development, Curr. Med. Chem. 18 (2011) 4738–4752, https://doi.org/10.2174/ 092986711707535308
- Z. Guo, P.J. Sadler, Metals in medicine, Angew. Chem. Int. Ed. 38 (1999) 1512–1531, https://doi.org/10.1002/(SICI)1521-3773(19990601)38:11<1512:: AID-ANIE1512>3.0.CO:2-Y.
- [8] F. Arnesano, G. Natile, Mechanistic insight into the cellular uptake and processing of cisplatin 30 years after its approval by FDA, Coord. Chem. Rev. 253 (2009) 2070–2081, https://doi.org/10.1016/j.ccr.2009.01.028.
- [9] M.A. Jakupec, M.S. Galanski, V.B. Arion, C.G. Hartinger, B.K. Keppler, Antitumour metal compounds: more than theme and variations, Dalton Trans. (2008) 183–194, https://doi.org/10.1039/B712656P.
- [10] B. Lippert, Cisplatin: chemistry and biochemistry of a leading anticancer drug (1999) 563.
- [11] A.D. Phillips, L. Gonsalvi, A. Romerosa, F. Vizza, M. Peruzzini, Coordination chemistry of 1,3,5-triaza-7-phosphaadamantane (PTA), Coord. Chem. Rev. 248 (2004) 955–993, https://doi.org/10.1016/j.ccr.2004.03.010.
- [12] K.J. Fisher, I.G. Dance, G.D. Willett, R. Zhang, E.C. Alyea, Electrospray studies of a water soluble platinum(II) phosphine complex, chlorotris(1,3,5-Triaza-7-Phosphaadamantane)platinum(II) chloride (TPA)₃PtCl₂, Eur. J. Mass Spectrom. 6 (2000) 23–30, https://doi.org/10.1255/ejms.315.
- [13] A. Guerriero, L. Gonsalvi, From traditional PTA to novel CAP: a comparison between two adamantane cage-type aminophosphines, Inorg. Chim. Acta 518 (2021) 120251, https://doi.org/10.1016/j.ica.2021.120251.
- [14] T. Lorenzon, M. Vescovo, M. Maiullari, G. Tonon, N.R. Conceição, S.A. C. Carabineiro, A.G. Mahmoud, M.C. Dietl, N. Demitri, L. Orian, P.A. Nogara, I. Caligiuri, F. Rizzolio, A.S.K. Hashmi, F. Visentin, T. Scattolin, Influence of the charge of 1,3,5-triaza-7-phosphaadamantane-based ligands on the anticancer activity of organopalladium complexes, RSC. Adv. 15 (2025) 14058–14071, https://doi.org/10.1039/d5ra02119g.
- [15] B. López-Sánchez, F. Scalambra, A. Romerosa, Transformation of the pheromone 3-methyl-2-cyclohexen-1-ol in the presence of [RuClCp(PTA)₂] and [RuCp(OH₂) (PTA)₂]CF₃SO₃, Appl. Organom. Chem. 38 (2024), https://doi.org/10.1002/aoc.7368.
- [16] P. Smoleński, U. Śliwińska-Hill, A. Kwiecień, J. Wolińska, D. Poradowski, Design, synthesis, and anti-cancer evaluation of novel water-soluble copper(I) complexes bearing terpyridine and PTA ligands, Molecules 29 (2024) 945, https://doi.org/10.3390/molecules29050945.
- [17] M.D. Živković, J. Kljun, T. Ilic-Tomic, A. Pavic, A. Veselinović, D.D. Manojlović, J. Nikodinovic-Runic, I. Turel, A new class of platinum(n) complexes with the phosphine ligand pta which show potent anticancer activity, Inorg. Chem. Front. 5 (2018) 39–53, https://doi.org/10.1039/C7Q100299H.
- [18] J. Braddock-Wilking, S. Acharya, N.P. Rath, Synthesis and characterization of Pt(II) and Pd(II) PTA and DAPTA complexes, Polyhedron 79 (2014) 16–28, https://doi.org/10.1016/j.poly.2014.04.040.
- [19] S.P. Sheelakumari, M.V. Cappellari, M.B. Rivas Aiello, A. Hepp, C.A. Strassert, Synthesis and photophysical evaluation of isoleptic Pt(II) and Pd(II) complexes utilizing N°N°N ligands as luminophoric chelators with different ancillary ligands, Inorganics 12 (2024) 58, https://doi.org/10.3390/inorganics12020058.
- [20] P. Smoleński, S. Mukhopadhyay, M.F.C. Guedes Da Silva, M.A.J. Charmier, A.J. L. Pombeiro, New water-soluble azido- and derived tetrazolato-platinum(ii) complexes with PTA. Easy metal-mediated synthesis and isolation of 5-substituted tetrazoles, Dalton. Trans. (2008) 6546, https://doi.org/10.1039/b808156e.
- [21] E. Guerrero, S. Miranda, S. Lüttenberg, N. Fröhlich, J.-M. Koenen, F. Mohr, E. Cerrada, M. Laguna, A. Mendía, trans-thionate derivatives of Pt(II) and Pd(II) with water-soluble phosphane PTA and DAPTA ligands: antiproliferative activity against Human ovarian cancer cell lines, Inorg. Chem. 52 (2013) 6635–6647, https://doi.org/10.1021/ic4006746.
- [22] E.C. Alyea, G. Ferguson, S. Kannan, Some water-soluble organometallic complexes of group 10 transition metal (II) ions with 1,3,5-triaza-7-phosphaadamantane (TPA). Syntheses, characterization and reactivity. The crystal and molecular structure of [Ni(CN)₂(TPA)₃]·3H₂O, Polyhedron 17 (1998) 2727–2732, https:// doi.org/10.1016/S0277-5387(98)00055-2.
- [23] S. Otto, A. Roodt, W. Purcell, Synthesis and characterisation of water soluble Pt(II) complexes of 1,3,5-triaza-7-phosphaadamantane (PTA). Crystal and molecular structure of {cis-[PtCl₂(PTA)₂]}₂ · H₂O, Inorg. Chem. Commun. 1 (1998) 415–417, https://doi.org/10.1016/S1387-7003(98)00106-3.
- [24] D.A. Krogstad, S.B. Owens, J.A. Halfen, V.G. Young, Intramolecular hydroamination of alkynylamines in aqueous media catalyzed by platinum(II)

- 1,3,5-triaza-7-phosphaadamantane (PTA) complexes, Inorg. Chem. Commun. 8 (2005) 65–69, https://doi.org/10.1016/j.inoche.2004.11.006.
- [25] D.A. Krogstad, J. Cho, A.J. DeBoer, J.A. Klitzke, W.R. Sanow, H.A. Williams, J. A. Halfen, Platinum(II) and palladium(II) 1,3,5-triaza-7-phosphaadamantane (PTA) complexes as intramolecular hydroamination catalysts in aqueous and organic media, Inorg. Chim. Acta 359 (2006) 136–148, https://doi.org/10.1016/j.ica.2005.08.028
- [26] M.Y. Demakova, K.V. Luzyanin, G.L. Starova, V.Y. Kukushkin, Facile alternative route to cis-[PtCl₂(PTA)₂] and [PtCl(PTA)₃]Cl (PTA = 1,3,5-triaza-7phosphaadamantane), Inorg. Chem. Commun. 50 (2014) 17–18, https://doi.org/ 10.1016/i.inoche.2014.10.002.
- [27] A.K. Renfrew, A.D. Phillips, A.E. Egger, C.G. Hartinger, S.S. Bosquain, A. A. Nazarov, B.K. Keppler, L. Gonsalvi, M. Peruzzini, P.J. Dyson, Influence of structural variation on the anticancer activity of RAPTA-type complexes: ptn versus pta, Organometallics 28 (2009) 1165–1172, https://doi.org/10.1021/om800899e.
- [28] C.A. Mebi, B.J. Frost, Isomerization of trans-[Ru(PTA)₄Cl₂] to cis-[Ru(PTA)₄Cl₂] in water and organic solvent: revisiting the chemistry of [Ru(PTA)₄Cl₂], Inorg. Chem. 46 (2007) 7115–7120, https://doi.org/10.1021/ic700971n.
- [29] F. Mohr, S. Sanz, E.R.T. Tiekink, M. Laguna, Water-soluble and Water-stable organometallic gold(II) complexes, Organometallics 25 (2006) 3084–3087, https://doi.org/10.1021/om0602456.
- [30] F. Mohr, E. Cerrada, M. Laguna, Organometallic gold(I) and gold(III) complexes containing 1,3,5-triaza-7-phosphaadamantane (TPA): examples of water-soluble Organometallic gold compounds, Organometallics 25 (2006) 644–648, https://doi. org/10.1021/org/508524
- [31] S. Miranda, E. Vergara, F. Mohr, D. de Vos, E. Cerrada, A. Mendía, M. Laguna, Synthesis, characterization, and in vitro cytotoxicity of some gold(I) and trans platinum(II) thionate complexes containing water-soluble PTA and DAPTA ligands. X-ray crystal structures of [Au(SC₄H₃N₂)(PTA)], trans-[Pt(SC₅H₄N)₂(PTA)₂], and trans-[Pt(SC₅H₄N)₂(DAPTA)₂], Inorg. Chem. 47 (2008) 5641–5648, https://doi.org/10.1021/ic7021903.
- [32] M. Werner, C. Bruhn, D. Steinborn, From platina-β-diketones to diacetylplatinum (II) complexes – Synthesis, characterization and structural features, J. Organomet. Chem. 693 (2008) 2369–2376, https://doi.org/10.1016/j. jorganchem.2008.04.016.
- [33] M. Gerisch, F.W. Heinemann, C. Bruhn, J. Scholz, D. Steinborn, Reactivity of dinuclear platina-β-diketones toward phosphines and pyridines: formation of mononuclear platina-β-diketones and acyl(chloro)platinum(II) complexes, Organometallics 18 (1999) 564–572, https://doi.org/10.1021/om980793m.
- [34] G.M. Sheldrick, IUCr, SHELXT Integrated space-group and crystal-structure determination, Acta Crystallographica Section A Foundat. Adv. 71 (2015) 3–8, https://doi.org/10.1107/S2053273314026370.
- [35] M.J. Turner, J.J. McKinnon, S.K. Wolff, D.J. Grimwood, P.R. Spackman, D. Jayatilaka, M.A. Spackman, CrystalExplorer 17, (2017).
- [36] M.A. Spackman, P.G. Byrom, A novel definition of a molecule in a crystal, Chem. Phys. Lett. 267 (1997) 215–220, https://doi.org/10.1016/S0009-2614(97)00100-
- [37] M.A. Spackman, D. Jayatilaka, Hirshfeld surface analysis, Cryst. Eng. Comm. 11 (2009) 19–32, https://doi.org/10.1039/B818330A.
- [38] M.J. Frisch, G.W. Trucks, H.B. Schlegel, G.E. Scuseria, M.A. Robb, J.R. Cheeseman, G. Scalmani, V. Barone, B. Mennucci, G.A. Petersson, H. Nakatsuji, M. Caricato, X. Li, H.P. Hratchian, A.F. Izmaylov, J. Bloino, G. Zheng, J.L. Sonnenberg, M. Hada, M. Ehara, K. Toyota, R. Fukuda, J. Hasegawa, M. Ishida, T. Nakajima, Y. Honda, O. Kitao, H. Nakai, T. Vreven, J.A. Montgomery Jr., J.E. Peralta, F. Ogliaro, M. Bearpark, J.J. Heyd, E. Brothers, K.N. Kudin, V.N. Staroverov, R. Kobayashi, J. Normand, K. Raghavachari, A. Rendell, J.C. Burant, S.S. Iyengar, J. Tomasi, M. Cossi, N. Rega, J.M. Millam, M. Klene, J.E. Knox, J.B. Cross, V. Bakken, C. Adamo, J. Jaramillo, R. Gomperts, R.E. Stratmann, O. Yazyev, A.J. Austin, R. Cammi, C. Pomelli, J.W. Ochterski, R.L. Martin, K. Morokuma, V.G. Zakrzewski, G.A. Voth, P. Salvador, J.J. Dannenberg, S. Dapprich, A.D. Daniels, Ö. Farkas, J. B. Foresman, J.V. Ortiz, J. Cioslowski, D.J. Fox, Gaussian 09. http://www.gaussian.com, 2009.
- [39] A.D. Becke, Density-functional thermochemistry. III. The role of exact exchange, J. Chem. Phys. 98 (1993) 5648, https://doi.org/10.1063/1.464913.
- [40] T.H. Dunning, Gaussian basis sets for use in correlated molecular calculations. I. The atoms boron through neon and hydrogen, J. Chem. Phys. 90 (1989) 1007, https://doi.org/10.1063/1.456153.
- [41] W.R. Wadt, P.J. Hay, Ab initio effective core potentials for molecular calculations. Potentials for main group elements Na to Bi, J. Chem. Phys. 82 (1985) 284–298, https://doi.org/10.1063/1.448800
- [42] D.S. Mohamed, S.A. Al-Jibori, R. Behjatmanesh-Ardakani, A.S. Faihan, T.A. Yousef, A.G. Alhamzani, M.M. Abou-Krisha, A.S.M. Al-Janabi, B.S. Hsiao, Spectroscopic, anti-cancer activity, and DFT computational studies of Pt(II) complexes with 1-benzyl-3-phenylthiourea and phosphine/diamine ligands, Inorganics 11 (2023) 1–15, https://doi.org/10.3390/inorganics11030125.
- [43] M. Sankarganesh, R.V. Solomon, J.D. Raja, Platinum complex with pyrimidine- and morpholine-based ligand: synthesis, spectroscopic, DFT, TDDFT, catalytic reduction, in vitro anticancer, antioxidant, antimicrobial, DNA binding and molecular modeling studies, J. Biomol. Struct. Dynamics 39 (2021) 1055–1067, https://doi.org/10.1080/07391102.2020.1727364.
- [44] A.V. Marenich, C.J. Cramer, D.G. Truhlar, Universal solvation model based on solute electron density and on a continuum model of the solvent defined by the bulk dielectric constant and atomic surface tensions, J. Phys. Chem. B 113 (2009) 6378–6396, https://doi.org/10.1021/jp810292n.

- [45] K. Wolinski, J.F. Hinton, P. Pulay, Efficient implementation of the gauge-independent atomic orbital method for NMR chemical shift calculations, J. Am. Chem. Soc. 112 (1990) 8251–8260, https://doi.org/10.1021/ja00179a005.
- [46] R. Ditchfield, Self-consistent perturbation theory of diamagnetism, Mol. Phys. 27 (1974) 789–807, https://doi.org/10.1080/00268977400100711.
- [47] R.F.W. Bader, Atoms in molecules, Acc. Chem. Res. 18 (1985) 9–15, https://doi. org/10.1021/ar00109a003.
- [48] R.F.W. Bader, T.S. Slee, D. Cremer, E. Kraka, Description of conjugation and hyperconjugation in terms of electron distributions, J. Am. Chem. Soc. 105 (1983) 5061–5068, https://doi.org/10.1021/ja00353a035.
- [49] M. Hesse, H. Meier, B. Zeeh, Spektroskopische Methoden in Der Organischen Chemie, 7th editio, Georg Thieme Verlag, 2002.
- [50] J. Vicente, A. Arcas, M.-D. Gálvez-López, P.G. Jones, Bis(2,6-dinitroaryl)platinum (II) complexes. Cis/trans isomerization, Organometallics 25 (2006) 4247–4259, https://doi.org/10.1021/om060398t.
- [51] L.M. Rendina, R.J. Puddephatt, Oxidative addition reactions of organoplatinum(II) complexes with nitrogen-donor ligands, Chem. Rev. 97 (1997) 1735–1754, https://doi.org/10.1021/cr9704671.
- [52] H.G. Alt, R. Baumgärtner, H.A. Brune, Über die konfigurations- und substituentenabhängigkeit der Pt ♦ Cl-valenzschwingungsfrequenzen und der ³¹P-NMRparameter in substituierten cis- und trans-dichlorobis-(triphenylphosphan)platin (II)-verbindungen, Chem. Ber. 119 (1986) 1694–1703, https://doi.org/10.1002/ cber.19861190521.
- [53] T.G. Appleton, H.C. Clark, L.E. Manzer, The trans-influence: its measurement and significance, Coord. Chem. Rev. 10 (1973) 335–422, https://doi.org/10.1016/ S0010-8545(00)80/38-6
- [54] H.A. Bent, Structural chemistry of donor-acceptor interactions, Chem. Rev. 68 (1968) 587–648, https://doi.org/10.1021/cr60255a003.
- [55] C. Albrecht, Dissertation, Martin-Luther-Universität Halle-Wittenberg, 2007.
- [56] A. Okuniewski, D. Rosiak, J. Chojnacki, B. Becker, Coordination polymers and molecular structures among complexes of mercury(II) halides with selected 1benzoylthioureas, Polyhedron 90 (2015) 47–57, https://doi.org/10.1016/j. poly.2015.01.035.
- [57] C. Albrecht, C. Wagner, D. Steinborn, Zur reaktivität von dinuklearen platinaβ-diketonen gegenüber phosphanen: diacetylplatin(II)-komplexe und mononukleare platina-β-diketone, Z. Anorg. Allg. Chem. 634 (2008) 2858–2866, https://doi.org/10.1002/zaac.200800317.
- [58] D. Steinborn, T. Hoffmann, M. Gerisch, C. Bruhn, H. Schmidt, K. Nordhoff, J. A. Davies, K. Kirschbaum, I. Jolk, On the reactivity of platina-β-diketones synthesis and characterization of acylplatinum(II) complexes, Z. Anorg. Allg. Chem. 626 (2000) 661–666, https://doi.org/10.1002/(SICI)1521-3749(200003) 626:3<661::AID-ZAAC661>3.0.CO;2-4.
- [59] M. Block, M. Bette, C. Wagner, D. Steinborn, On the reactivity of the platina-β-diketone [Pt₂{(COMe)₂H₂(μ-Cl)₂] towards Ph₂PCH₂CH₂CH₂SO_xPh (x = 0, 2), Z. Anorg. Allg. Chem. 637 (2011) 206–210, https://doi.org/10.1002/zaac.201000344.
- [60] G.A. Jeffrey, An Introduction to Hydrogen Bonding, Oxford University Press, 1997.
- [61] J. Moto Ongagna, A.D. Tamafo Fouegue, B. Ateba Amana, G. Mouzong D'ambassa, J. Zobo Mfomo, L. Mbaze Meva'A, D. Bikele Mama, B3LYP, M06 and B3PW91 DFT assignment of nd⁸ metal-bis-(N-heterocyclic carbene) complexes, J. Mol. Model. 26 (2020) 246, https://doi.org/10.1007/s00894-020-04500-7.
- [62] İ. Yılmaz, N. Acar-Selçuki, S.J. Coles, F. Pekdemir, A. Şengül, Spectroscopic, structural and DFT studies of luminescent Pt(II) and Ag(I) complexes with an asymmetric 2,2'-bipyridine chelating ligand, J. Mol. Struct. 1223 (2021) 129271, https://doi.org/10.1016/j.molstruc.2020.129271.
- [63] M.P. Kasalović, S. Jelača, Ž. Milanović, D. Maksimović-Ivanić, S. Mijatović, J. Ladarević, B. Božić, Z. Marković, D. Dunđerović, T. Rüffer, R. Kretschmer, G. N. Kaluđerović, N.D. Pantelić, Novel triphenyltin(IV) compounds with carboxylato N-functionalized 2-quinolones as promising potential anticancer drug candidates: in vitro and in vivo evaluation, Dalton Trans. 53 (2024) 8298–8314, https://doi.org/10.1039/D4DT00182F.
- [64] M.P. Kasalović, S. Jelača, D. Dimić, D. Maksimović-Ivanić, V.V. Jevtić, S. Mijatović, T. Rüffer, G.N. Kaluđerović, N.D. Pantelić, Organic moiety on Sn(IV) does matter for *In vitro* mode of action: nBu₃Sn(IV) compounds with carboxylato N-functionalized 2-quinolones induce anoikis-like cell death in A375 cells, Pharmaceutics 16 (2024) 1529, https://doi.org/10.3390/pharmaceutics16121529.
- [65] Y. Li, G. Zhang, D. Chen, Theoretical investigation of hydrogen bonding between water and platinum(II): an atom in molecule (AIM) study, Mol. Phys. 110 (2012) 179–184, https://doi.org/10.1080/00268976.2011.637522.
- [66] S.M. Soliman, J. Albering, M.A.M. Abu-Youssef, Structural analyses of two new highly distorted octahedral copper(II) complexes with quinoline-type ligands; Hirshfeld, AIM and NBO studies, Polyhedron 127 (2017) 36–50, https://doi.org/ 10.1016/j.poly.2017.01.051.
- [67] C. Lepetit, B. Vabre, Y. Canac, M.E. Alikhani, D. Zargarian, Pentacoordinated, square pyramidal cationic PCP Ni(II) pincer complexes: ELF and QTAIM topological analyses of nickel-triflate interactions, Theor. Chem. Acc. 137 (2018) 141, https://doi.org/10.1007/s00214-018-2332-y.
- [68] R. Bianchi, G. Gervasio, D. Marabello, Experimental electron density analysis of Mn 2 (CO) 10: metal—metal and metal—ligand bond characterization, Inorg. Chem. 39 (2000) 2360–2366, https://doi.org/10.1021/ic991316e.
- [69] E. Espinosa, E. Molins, C. Lecomte, Hydrogen bond strengths revealed by topological analyses of experimentally observed electron densities, Chem. Phys. Lett. 285 (1998) 170–173, https://doi.org/10.1016/S0009-2614(98)00036-0.
- [70] Á.B. Cruz, A.K. dos Santos Pereira, D.H. Pereira, Structural and electronic analysis of sulfonamide coordination with platinum: a density functional theory study, Russ

- J. Coord. Chem. 50 (2024) 1008-1028, https://doi.org/10.1134/ S1070328424601109.
- [71] M. Bayat, F. Yaghoobi, S. Salehzadeh, S. Hokmi, A theoretical study on the interaction of $[Al(H_2O)_6]^{3+}$ and $[Mg(H_2O)_6]^{2+}$ cations with fullerene (C60), coronene and benzene π -systems, Polyhedron 30 (2011) 2809–2814, https://doi. org/10.1016/j.poly.2011.08.017.
- [72] U. Koch, P.L.A. Popelier, Characterization of C-H-O hydrogen bonds on the basis of the charge density, J. Phys. Chem. 99 (1995) 9747-9754, https://doi.org/ 10.1021/j100024a016.
- [73] K. Szmigiel-Bakalarz, M. Nentwig, O. Oeckler, M. Malik-Gajewska, B. Filip-Psurska, B. Morzyk-Ociepa, 7-Azaindole-3-carboxylic acid and its Pt(II) and Pd(II) complexes: crystal structure of the ligand, vibrational spectra, DFT calculations and in vitro antiproliferative activity, J. Mol. Struct. 1203 (2020) 127441, https://doi. org/10.1016/j.molstruc.2019.127441.

 [74] B. Lu, X. Zhang, L. Meng, Y. Zeng, The Pt (II)···Cl interactions: nature and strength,
- Chem. Select. 1 (2016) 5698-5705, https://doi.org/10.1002/slct.201601230.